PHILOSOPHICAL TRANSACTIONS OF THE ROYAL SOCIETY B BIOLOGICAL SCIENCES

Neuronal rebound spiking, resonance frequency and theta cycle skipping may contribute to grid cell firing in medial entorhinal cortex

Michael E. Hasselmo

Phil. Trans. R. Soc. B 2014 **369**, 20120523, published 23 December 2013

PHILOSOPHICAL TRANSACTIONS OF THE ROYAL SOCIETY B

rstb.royalsocietypublishing.org

Research

Cite this article: Hasselmo ME. 2014 Neuronal rebound spiking, resonance frequency and theta cycle skipping may contribute to grid cell firing in medial entorhinal cortex. *Phil. Trans. R. Soc. B* **369**: 20120523.
http://dx.doi.org/10.1098/rstb.2012.0523

One contribution of 24 to a Theo Murphy Meeting Issue 'Space in the brain: cells, circuits, codes and cognition'.

Subject Areas:
neuroscience, behaviour, cognition, physiology, theoretical biology

Keywords:
grid cells, head direction, place cells, entorhinal cortex, rat, theta rhythm

Author for correspondence:
Michael E. Hasselmo
e-mail: hasselmo@bu.edu

Electronic supplementary material is available at http://dx.doi.org/10.1098rstb.2012.0523 or via http://rstb.royalsocietypublishing.org.

Royal Society Publishing

Neuronal rebound spiking, resonance frequency and theta cycle skipping may contribute to grid cell firing in medial entorhinal cortex

Michael E. Hasselmo

Center for Memory and Brain, Department of Psychology and Graduate Program for Neuroscience, Boston University, 2 Cummington St., Boston, MA 02215, USA

Data show a relationship of cellular resonance and network oscillations in the entorhinal cortex to the spatial periodicity of grid cells. This paper presents a model that simulates the resonance and rebound spiking properties of entorhinal neurons to generate spatial periodicity dependent upon phasic input from medial septum. The model shows that a difference in spatial periodicity can result from a difference in neuronal resonance frequency that replicates data from several experiments. The model also demonstrates a functional role for the phenomenon of theta cycle skipping in the medial entorhinal cortex.

1. Introduction

Experimental data show correlations of grid cell firing with intrinsic resonance properties of medial entorhinal neurons, but previous models have not directly addressed resonance. A model presented here attempts to link resonance properties to grid cell firing by using network dynamics dependent upon timing of rebound depolarization causing rebound spiking activity. In the model, the phase of rebound spiking relative to the phase of rhythmic input from medial septum determines which neurons next become active, resembling the oscillatory interference model of grid cells. Transitions between active neurons can be regulated by changes in inhibition input magnitude or medial septum frequency associated with running velocity, resulting in spatially periodic firing similar to grid cells. When inhibition is used to generate rebound spiking, maintenance of network activity can use alternating cycles of input activity that resemble data on theta cycle skipping by neurons in medial entorhinal cortex and medial septum. Loss of medial septal input causes loss of spatially periodic firing. The model requires updating the phase of input from medial septum similar to the ring attractor model of grid cells. The model potentially links differences in intrinsic resonance properties to changes in grid cell firing properties in different anatomical recording locations.

Grid cells generate spikes as an animal visits an array of locations in the environment that fall on the vertices of equilateral triangles tessellating the environment [1,2]. A number of models address the mechanism of grid cell firing, and different models successfully account for different aspects of the spatial firing properties. Oscillatory interference models [3–7] address the theta rhythmic firing of grid cells [8–12], the theta phase precession of grid cells [8,13] and the prominent theta in the local field potential of entorhinal cortex [14–17]. Attractor models [18–21] address the shared orientation and spacing of grid cell firing fields [22] and the quantal spacing of grid cell firing fields [12,23]. Self-organization models [24–26] can account for the loss of grid cell firing with inactivation of the hippocampus [27]. Researchers often contrast models using oscillatory interference with those using attractor dynamics or self-organization, but many features of these models are compatible and could coexist within a single network model of grid cells.

However, the simplified structure of most existing models does not address the full range of physiological data. In particular, most models do not incorporate

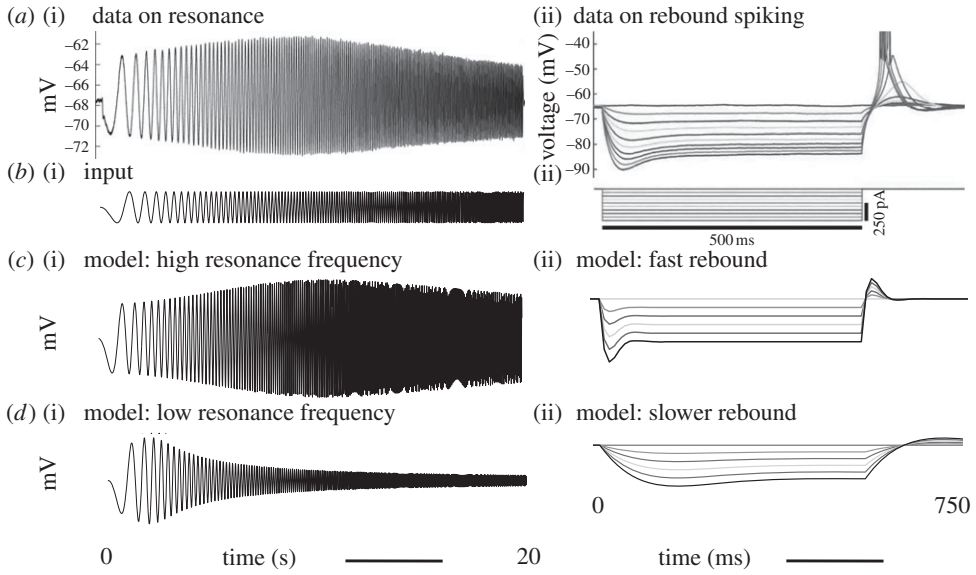

Figure 1. (*a*(i)) Experimental data showing the membrane potential of a layer II medial entorhinal cortex stellate cell during resonance testing (data in (*a*(i)(ii)) gathered by Shay [37]). In response to oscillating current injection that increases in frequency, the neuron shows a gradual increase in amplitude of membrane potential deflection that reaches a peak at resonance frequency, and then decreases. (*b*(i)) The chirp function input to (*a*(i)) sweeps from 0 to 20 Hz over a period of 20 s. (*c*(i)) A simulated stellate cell using equation (4.1) shows the same theta frequency resonance in response to the chirp function, with $g_p = 0.75$, $g_h = 0.15$ and $o_h = 0.35$. (*d*(i)) A simulated cell with a different parameter $g_p = 0.109$, $g_h = 0.009$ and $o_h = 0.1$ shows resonance at lower frequency (1–2 Hz) similar to bats or mice with knockout of the HCN1 subunit. (*a*(ii)) Experimental data show the membrane potential of a layer II stellate cell during and after hyperpolarizing steps of different amplitude, showing the depolarizing sag during input, and the depolarizing rebound that generates spikes after input [37]. (*b*(ii)) Input to (*a*(ii)) showing hyperpolarizing steps. (*c*(ii)) A simulated stellate cell using the parameters in (*c*(i)) shows the same depolarizing sag during simulated current injection and depolarizing rebound afterward. (*d*(ii)) A simulated cell with parameters from (*d*(i)) still shows sag and rebound but on a slower time-scale.

intrinsic properties of neurons. The model presented in this article builds on previous models of grid cells, including the oscillatory interference model [3–5] and ring attractor model [6,28], but with a specific focus on addressing physiological data on intrinsic rebound spiking and theta cycle skipping not addressed by previous models. In particular, the model is motivated by the desire to address the correlation between grid cell properties and the presence and frequency of resonance in medial entorhinal neurons [29–37] and the potential functional role of rebound spiking of stellate cells owing to the hyperpolarization-activated cation current (*h* current) [37–39]. The model was also motivated by the phenomenon of theta cycle skipping observed in the spiking of neurons in the medial entorhinal cortex [17,40,41] and in the medial septum [42,43] and the loss of grid cell firing with inactivation of the medial septum [10,11].

2. Intracellular data on resonance

Physiological data using both intracellular and extracellular recording techniques provided the primary motivation for this new model. In particular, existing models do not satisfactorily link the firing of grid cells to the data on intracellular resonance [29–37] and rebound spiking [37–39] in layer II stellate cells as in the examples shown in figure 1*a*. The model has been developed in an attempt to address the frequently replicated data showing a difference in resonance frequency along the dorsal to ventral axis [31–34,37] that correlates with the size and spacing between grid cell firing fields [12,22,44]. The link with grid cell firing is supported by the appearance of resonance in layer II stellate cells in medial entorhinal cortex [29,35–37] but not in layer II neurons in lateral entorhinal cortex, correlating with the unit recording data showing grid cells in medial but not lateral entorhinal cortex [45]. In addition, the model was motivated by data showing modulatory reductions in cellular resonance frequency by acetylcholine [46] and data on acetylcholine release in novel environments [47] that could underlie the difference in spacing observed in novel environments [48,49].

Simulations in the model also suggest how grid cell properties could still be generated by cells with very low resonance frequencies (1–2 Hz). This is relevant to data showing that knockout of the HCN1 subunit of the *h* current that results in only very low frequency resonance in stellate cells [50] does not prevent the appearance of grid cell firing fields, but does expand the size and spacing of these firing fields [51]. Modelling with these low resonance frequencies also suggests how the low resonance frequency observed in slice preparations of entorhinal cortex in bats [52] could still underlie the generation of grid cells in the entorhinal cortex of crawling bats [53].

3. Extracellular data on theta cycle skipping and loss of theta rhythm

Many features of extracellular spiking activity have been successfully addressed by existing models, but some aspects of extracellular spiking data remain to be addressed. Attractor models have many strengths in effectively simulating population features of grid cells [18–21,54], including the shared spacing and orientation of nearby grid cells [8] and the quantal nature of these grid cell properties [12,23]. However, most attractor models do not yet address the theta rhythmic firing of grid cells that results in intervals between spikes that are often over 100 ms. Some existing grid cell models that simulate theta rhythmic spiking of neurons have used slow time

constants of synaptic potentials [55,56]. As an alternative to slow synaptic interactions, one attractor model overcame the problem of simulating long interspike intervals by using an alternative solution involving rebound spiking dependent on prior spikes [56]. That also allowed simulation of theta phase precession [56]. The model presented here also uses rebound spiking, but the rebound in this new model arises from subthreshold dynamics rather than previous spikes, allowing simulation of subthreshold resonance properties and of rebound spiking after hyperpolarization.

Oscillatory interference models simulate the firing field periodicity and theta phase precession [5] observed in data on grid cells [8,13], but do not yet use the phenomenon of theta cycle skipping observed in many medial entorhinal neurons [17,40,41] and in the medial septum [42,43]. Using mechanisms of rebound spiking, the model presented here will address both the functional role of theta cycle skipping as well as the long interspike intervals in theta rhythmic spiking. The model also indicates why grid cell spatial periodicity would be lost with inactivation of the medial septum [10,11].

4. Model using resonance and rebound spiking in medial entorhinal cortex

This model uses the physiological properties of resonance and rebound spiking in layer II stellate cells to reactivate population activity on each theta cycle. Stellate cells in medial entorhinal cortex are only present in layer II and contain a hyperpolarization-activated cation current (h current) that underlies resonance at theta frequency [29,31,46,50] and causes a depolarizing rebound spike following a hyperpolarizing current injection [37–39]. These effects are weak or absent in pyramidal cells in deeper layers [35,57].

The resonance of single neurons can be represented with coupled differential equations as shown in equations (4.1) and (4.2), where v represents the membrane potential of the stellate cell and h represents the h current. The variable v responds to current input I_{in}, decreases with the passive decay g_p proportional to v and increases with the magnitude of depolarization g_h owing to the h current. The variable h decreases in proportion to positive values of membrane potential v and with passive decay proportional to the parameter o_h multiplied by the current magnitude h. The variable h increases when the membrane potential v is negative (i.e. hyperpolarized) and the value of $-v$ is positive.

$$\frac{dv}{dt} = -g_p v + g_h h + I_{\text{in}} \tag{4.1}$$

and

$$\frac{dh}{dt} = -v - o_h h. \tag{4.2}$$

As shown in figure 1*c*,*d*, this allows simulation of subthreshold resonance properties of neurons as well as the rebound depolarization following hyperpolarization. These figures show how different resonance frequencies of neurons including high (10 Hz) and low (1.4 Hz) can be simulated by altering the parameters. This allows testing of the relationship between resonance frequency and network dynamics in the model. Other models have also previously simulated stellate cell resonance [30,58,59].

Figure 2 shows the connectivity of one version of the model and these details are briefly described here. In the model, the populations of stellate cells s interact with populations of interneurons i, allowing the intrinsic dynamics of stellate cells to interact with the dynamics of network feedback inhibition, as described in these equations:

$$\frac{dv_s}{dt} = -g_p v_s + g_h h_s - W_{si} H[v_i - \eta_i] + I_{\text{Sms}}, \tag{4.3}$$

$$\frac{dh_s}{dt} = -v_s - o_h h_s \quad \text{and} \tag{4.4}$$

$$v_i = \sum_s W_{is} H[v_s - \eta_s] + I_{\text{ms}} + I_{\text{hd}}(\theta(t) - \theta_{\text{pref}}), \tag{4.5}$$

where v_s represents membrane potential of each stellate cell with index s and h_s represents the activation of the h current in each stellate cell. $H[.]$ computes output using a Heaviside or step function (0 for $v_s < \eta$, 1 for $v_s > \eta$, where η_s is the stellate cell threshold). The variable v_i represents the membrane potentials of interneurons, which also generates output through a Heaviside function with threshold η_i. In some versions of the model (figures 2 and 3), the matrix W_{si} is an identity matrix, with each interneuron contacting one stellate cell and the matrix W_{is} provides connectivity from each stellate cell in a population to all interneurons within a single 'line' coding locations along the direction coded by head direction input. In another model version in figure 4, a stellate cell population (e.g. T1) sends output to a single interneuron that connects to an entire stellate cell population (e.g. T2) and vice versa. Each interneuron also receives depolarizing current input I_{hd} coding current head direction θ relative to the preferred head direction of that line θ_{pref}. This is meant to represent the role of conjunctive grid-by-head-direction cells in gating the interaction of grid cells with interneurons. For simplicity of simulations, the intervening excitatory cells are left out of the simulations and the selective activation of interneurons is obtained with selective head direction input.

In the version with identity matrix input from multiple interneurons, each interneuron also receives oscillatory input from the medial septum with different phases according to the equation: $I_{\text{ms}} = \mu \sin(2\pi f t + 2\pi(i/n))$, where f is the medial septal frequency, i is the interneuron index and n is the total number of interneurons along one 'line' of the model. In the spiking versions of the model described below, the stellate cells also received an input I_{Sms} that had the same equation as the medial septal input to the interneurons but was shifted by phase $3\pi/2$ and had a different magnitude μ. The initial activity in each simulation was activated by giving an initial hyperpolarizing input to the stellate cells, causing a depolarizing rebound that crossed threshold in the continuous firing rate version and generated a rebound spike in the spiking model described below.

The network dynamics depend on the resonant frequency determined by the parameters g_p, g_h, o_h of the above equations and the relationship of this resonant frequency to the frequency f of the medial septal input. When the resonant frequency was significantly different from the medial septal input, this caused a shift in activity between different neurons in the population as shown in figures 2–4. In figures 2–4, the different populations of stellate cells and interneurons active on different theta cycles are designated with the letters S (stellate) or I (interneuron) with different subscripts T1 and T2 (for theta cycle 1 and theta cycle 2). Individual cells are also given cell numbers within these populations. For example, $S_{T1}4$, is the fourth stellate cell in the population responding on theta cycle T1. The populations S_{T1} and S_{T2} differ only in connectivity and do not differ in intrinsic

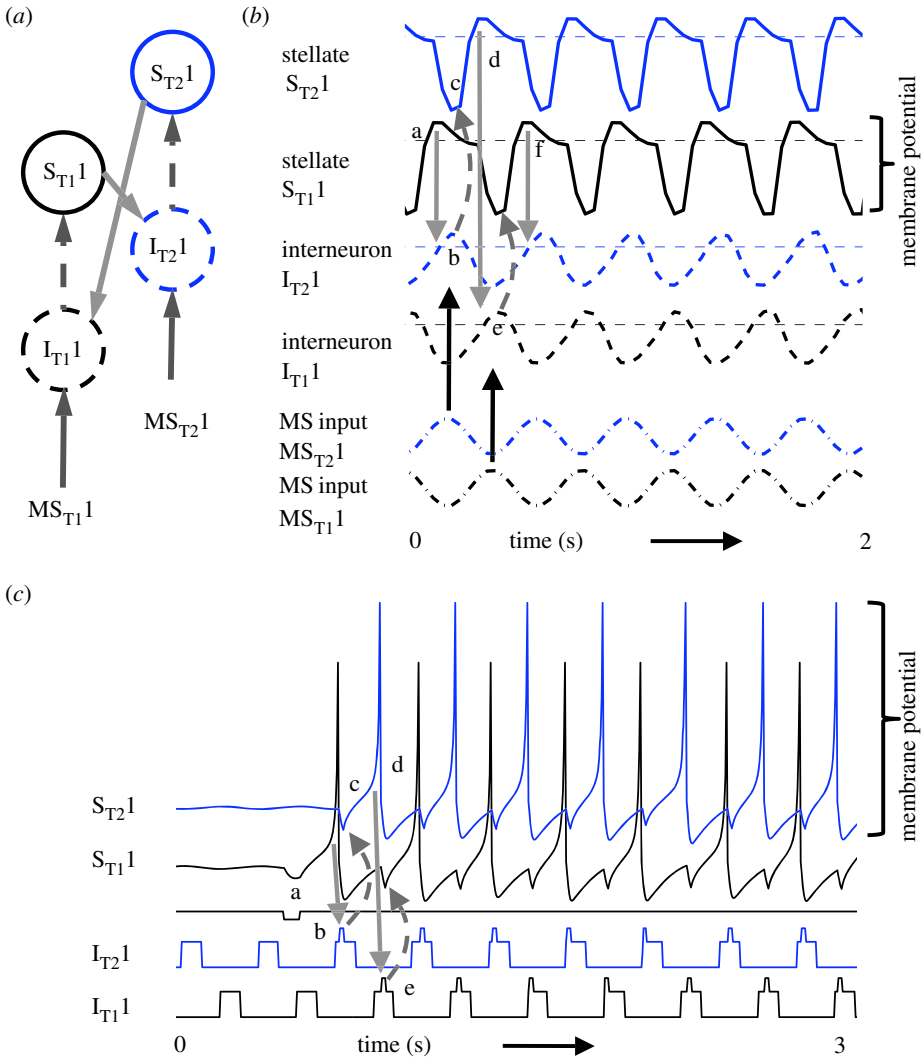

Figure 2. Sustained circuit activity with inhibitory feedback. (*a*) Local circuit showing excitatory connections (solid arrows) from stellate cell with index $S_{T1}1$ to interneuron with index $S_{T1}1$, and from stellate cell $S_{T2}1$ to interneuron $I_{T2}1$, and inhibitory connections (dashed arrows) from interneuron $I_{T1}1$ to stellate cell $S_{T1}1$ and from interneuron $I_{T2}1$ to stellate cell $S_{T2}1$. (*b*) Time course of change in activation of one coupled pair of cells: (step a) stellate cell $S_{T1}1$ (solid black line) starts out hyperpolarized, rebounds over the threshold shown by dotted line and sends excitatory synaptic output (grey line) to interneuron $I_{T2}1$; (step b) interneuron $I_{T2}1$ (dashed black line) is depolarized over threshold (thin dashed line); (step c) interneuron $I_{T2}1$ sends inhibitory output (grey dashed arrow) to cause hyperpolarization in stellate cell $S_{T2}1$ (top line); (step d) stellate cell $S_{T2}1$ rebounds from the hyperpolarization to cross threshold (thin dashed line), sending excitatory output to interneuron $I_{T1}1$; (step e) this brings interneuron $I_{T1}1$ over threshold, sending inhibitory output (grey dashed arrow) to hyperpolarize stellate cell $S_{T1}1$; (step f) this causes stellate $S_{T1}1$ to show rebound spiking to start the same cycle again. Bottom traces show that throughout this simulation, the interneurons $I_{T1}1$ and $I_{T2}1$ receive oscillatory medial septal (MS) input that determines when these interneurons are close to threshold and can generate spikes in response to stellate input. This example uses parameters as in figure 1*c*(i). (*c*) Example of spiking model with resonance using Izhikevich neurons. A hyperpolarizing pulse (label a) given to stellate cell $S_{T1}1$ causes a rebound spike. This brings interneuron $I_{T2}1$ above threshold by label b. The interneuron $I_{T2}1$ inhibits stellate cell $S_{T2}1$ (label c), causing a rebound spike (label d) that activates interneuron $I_{T1}1$ (label e). This causes an inhibitory potential in stellate cell $S_{T1}1$ to start the cycle again. Spikes fall on alternating cycles. (Online version in colour.)

properties. The interneuron populations I_{T1} and I_{T2} also differ only in connectivity and not in intrinsic properties.

As shown in figures 3 and 4, the resonance can alternatively be represented with a previously developed spiking model of medial entorhinal cortex stellate cell properties developed by Izhikevich [60] based on experimental data from Brian Burton in John White's laboratory. This model uses the following equations:

$$\left.\begin{aligned} C\dot{v} &= k(v - v_r)(v - v_t) - u + 1, \\ \dot{u} &= a\{b(v - v_r) - u\} \\ v &\geq v_{\text{peak}}, \quad v \leftarrow c, \quad u \leftarrow u + d. \end{aligned}\right\} \tag{4.6}$$

For stellate cells, the parameters were: $C = 200$, $v_r = -60$, $v_t = -45$, $v_{\text{peak}} = 30$, $k = 0.75$, $a = 0.01$, $b = 15$, $c = -50$ and $d = 100$. A difference in resonance frequency and rebound spiking was obtained by changing the parameter a from $a = 0.01$ to $a = 0.015$. These spiking stellate neurons interacted with the same abstract interneurons described above, but in the spiking model in figures 2*c* and 3 the medial septal input was structured as square wave inputs that did not overlap in the depolarized phase, so only one interneuron at a time was sufficiently depolarized to be able to respond to the synaptic input from the spiking stellate cells. Different directions of movement were represented by different sets of interneurons receiving tonic depolarizing input I_{hd} representing head direction input so that the stellate cells would interact only with interneurons receiving phasic input appropriate for the current heading direction. The phase of other interneurons would be updated

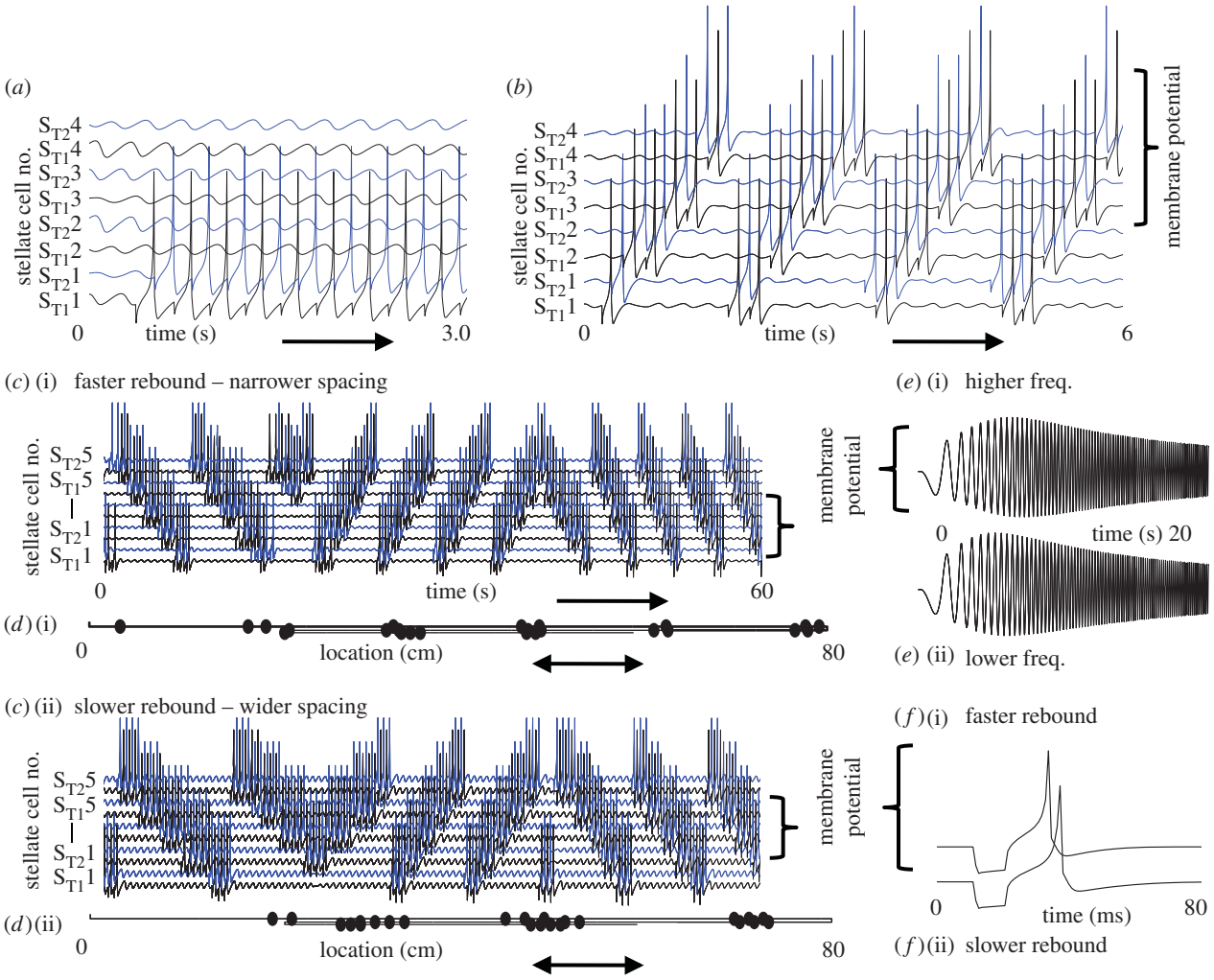

Figure 3. (*a*) Theta cycle skipping can remain stationary in stellate cells $S_{T1}1$ and $S_{T2}1$when rebound spiking matches the frequency of medial septal input to the interneurons (or when the interneurons get constant input). (*b*) Alternatively, the rebound spiking activity can shift between different stellate cells when the rebound spiking is faster than the period of oscillatory medial septal input to the interneurons. The shift is proportionate to the difference in frequency of resonance (rebound speed) and the frequency of medial septal input. (*c*) The rebound spiking can shift back and forth in a one-dimensional line of stellate cells when directional heading shifts from west (start) to east and back again with a corresponding shift in active interneurons with different phase distributions. The shift accelerates over time owing to a progressive increase in running speed. (*c*(i)) The shift is faster for cells with higher resonance frequency (*e*(i)) and faster rebound spiking (*f*(i)). The shift is slower for cells with lower resonance frequency (*e*(ii)) and slower rebound spiking (*f*(ii)). (*d*) The activity in (*c*) is plotted to show location of the rat (black dots) at the time of each spike generated by stellate cell $S_{T1}4$ (seventh line from bottom in figure 3*c*), showing firing in regular spatial locations as the rat runs back and forth along a linear track at different speeds (going different distances). (*d*(i)) Firing fields are closer together for cells with higher resonance frequency (*e*(i)) and faster rebound spiking (*f*(i)). (*d*(ii)) Firing fields are further apart for cells with lower resonance frequency (*e*(ii)) and slower rebound spiking (*f*(ii)). (Online version in colour.)

consistently so that at a turning location, the stellate activity could transition to interacting with an interneuron with the correct connectivity and phase to allow movement in the opposite direction. Thus, the update of position owing to rebound spiking needs to interact with phase reset of cells responding to other directions, consistent with previous oscillatory interference models [5] and ring attractor models [6,28,61]. In figure 4, a single interneuron received output from a full stellate cell population (e.g. T1) and provided inhibitory input to the opposite population (e.g. T2), and another single interneuron performed the opposite operation (from T2 to T1).

5. Periodicity with both high and low resonance frequencies

The model demonstrates that spatial periodicity could be generated by neurons with a range of different resonance frequencies. Figure 2*a* shows the circuit connectivity in which stellate cells with rebound depolarization interact with interneurons that get rhythmic medial septal input. Figure 2*b* shows the model from equations (4.1)–(4.5) using simulated stellate cells with parameters that match a typical stellate cell in rat dorsal medial entorhinal cortex [31,37] as shown in figure 1*c*(i)(ii). Figure 2*b* demonstrates the capacity of this circuit to maintain activity owing to the fact that stellate cells show rebound depolarization following hyperpolarizing inhibition. In this figure, the cycle time between rebound depolarizations of the stellate cells takes the same time interval as the medial septal input, so the activity stays stationary. Figure 2*c* shows the same effect with spiking neurons and will be described in §6.

In figure 2*b*, the activity starts out with an initial hyperpolarization in a stellate cell that causes depolarizing rebound (labelled as step a) that brings the stellate cell with index $S_{T1}1$ over threshold (dotted line). This causes excitatory synaptic

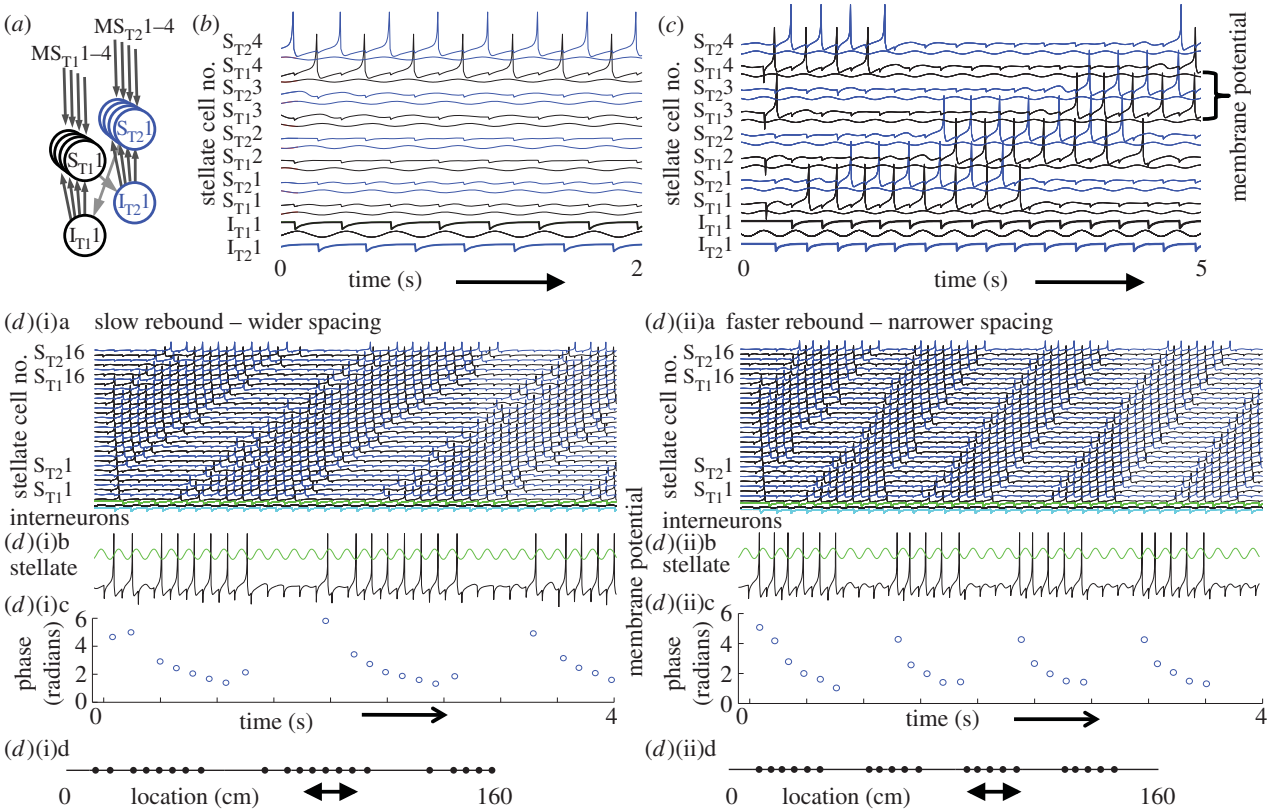

Figure 4. (*a*) Circuit design using oscillating medial septal (MS) input with different phases to two populations of stellate cells. Stellate cells interact with a single pair of interneurons that send inhibition to all stellate cells and cause rebound spiking in a subset of stellate cells. (*b*) Theta cycle skipping remains stationary in a subset of stellate cells $S_{T1}4$ and $S_{T2}4$ when rebound spiking matches the frequency of MS input to the stellate cells. For each cell, thick line shows membrane potential and thin line underneath shows MS input. Interneurons show strong feedback inhibition after each output spike. (*c*) Rebound spiking activity shifts between different stellate cells when rebound spiking is faster than the period of oscillatory MS input to the stellate cells. (*d*(i)a) In a larger population, the rebound spiking occurs in a subset of stellate cells and shifts progressively across the population. The spikes of an individual stellate cell (*d*(i)b) show theta phase precession relative to the medial septal frequency input (*d*(i)c). The spacing of firing fields is broad (*d*(i)d) when slow rebound spiking is only slightly faster than the medial septal input period. (*d*(ii)a) With faster rebound spiking, the difference from the period of medial septal input oscillations is larger. The spiking of individual cells (*d*(ii)b) shows faster theta phase precession (*d*(ii)c) and the size and spacing of firing fields are smaller (*d*(ii)d). (Online version in colour.)

output from the stellate cell to interneuron $I_{T2}1$ (step b). This synaptic input arrives at the peak of the oscillating input from medial septum $I_{T2}1$ to the same interneuron, allowing it to cross threshold (thin dashed line). Interneuron $I_{T2}1$ then sends synaptic inhibition (dashed line) to cause hyperpolarization in stellate cell $S_{T2}1$ (step c). Stellate cell $S_{T2}1$ subsequently shows a depolarizing rebound (step d) that brings it over threshold, causing excitatory synaptic output to interneuron $I_{T1}1$ (step e). This arrives at the peak of the oscillatory medial septal input allowing interneuron $I_{T1}1$ to cross threshold and cause inhibitory synaptic output to the first stellate cell $S_{T1}1$ (step f). In this manner, the self-sustaining cycle repeats itself, maintaining activity. The activity is stable in this example because the frequency of stellate cell rebound depolarization matches the medial septal input frequency.

If the timing of rebound depolarization differs from the interval determined by medial septum input frequency, then the activity can shift between different cells as shown in the electronic supplementary material, figure S1. In the example in the electronic supplementary material, figure S1, the activity shifts because the rebound spiking is faster than the frequency of input from the medial septum. Electronic supplementary material, figure S1A–C separately shows the populations of stellate cells (A), interneurons (B) and medial septal input (C). The medial septal input to each interneuron differs in phase. For example, the input to interneuron $I_{T2}2$ is earlier in phase (earlier peak) than the input to interneuron $I_{T2}1$. In addition to the medial septum input, each interneuron $I_{T2}1$–$I_{T2}5$ also receives excitatory synaptic input from every stellate cell $S_{T2}1$–$S_{T2}5$, but sends synaptic inhibition only to one stellate cell (interneuron $I_{T2}1$ to stellate $S_{T2}1$, interneuron $I_{T2}2$ to stellate $S_{T2}2$, etc.) via an identity matrix. At time 0 in the electronic supplementary material, figure S1, a subset of cells $S_{T2}1$–$S_{T2}4$ and $S_{T1}1$–$S_{T1}4$ are oscillating strongly. However, because the rebound is slightly faster than the medial septal frequency, the rebound occurs at an earlier phase, causing activation of an interneuron receiving medial septal input with earlier phase. This causes suprathreshold activation of interneurons $I_{T2}5$ and $I_{T1}5$ which hyperpolarize stellate cells $S_{T2}5$ and $S_{T1}5$, causing a further shift in the dominant phase of stellate activity. This results in neurons $I_{T2}1$ and $S_{T1}1$ falling below threshold and becoming inactive. This pattern continues, causing a sequential progression of oscillatory activity through the network. Eventually, the activity cycles back from $S_{T2}5$ and $S_{T1}5$ to $S_{T2}1$ and $S_{T1}1$, because $S_{T2}1$ and $S_{T1}1$ are at an earlier phase relative to $S_{T2}5$ and $S_{T1}5$.

The model also addresses recent data showing lack of resonance at theta frequency in layer II neurons in bat entorhinal cortex [52]. Instead of theta frequency, these neurons show resonance frequency between 1 and 2 Hz. To address these data, electronic supplementary material, figure S1 (parts

A,B,C) shows the circuit simulated using parameters matching the slower resonance frequency of a cell in bat medial entorhinal cortex [52], as simulated in figure 1*d*(i)(ii). For comparison, electronic supplementary material, figure S1 part D shows the circuit model with the parameters of theta frequency resonance from figure 2 (and figure 1*c*(i)(ii)) that match rat dorsal medial entorhinal cortex [31,37]. The models show the same functional ability to switch between different phases of activity, as long as the frequency of medial septal input is altered to be close to the frequency based on the intervals between rebound depolarizations. The main difference is that both the resonant frequency and medial septum frequency are faster in part D than in parts A, B and C. The same simulation could address the data showing loss of theta frequency resonance in layer II stellate cells in mice with knockout of the HCN1 subunit of the *h* current, because neurons in slices from the HCN1 knockout mice also show resonance in the range 1–2 Hz [50].

6. Rebound from inhibition can underlie sustained activity with theta cycle skipping

As shown in figures 2 and 3, the use of rebound from inhibition specifically uses the property of different neurons firing on alternating cycles of theta rhythm oscillations. This provides a functional rationale for the presence of theta cycle skipping in neurons of the medial entorhinal cortex [17,40,41]. The simulations in figures 2 and 3 use the synaptic connectivity structure shown in figure 2*a*, demonstrating the specific connectivity required for inhibitory rebound. To better simulate the role of theta cycle skipping [17,40,41], figure 2*c* shows the effect with simulations of individual medial entorhinal stellate cells that generate spikes using the Izhikevich model [60] described in §4. In figure 2*c*, simulated activity is initiated by a hyperpolarizing input to stellate cell $S_{T1}1$ (label a). This causes a rebound spike in stellate cell $S_{T1}1$ that activates an associated interneuron $I_{T2}1$ (label b). The interneuron $I_{T2}1$ inhibits a separate stellate cell $S_{T2}1$, causing hyperpolarization (label c) that induces rebound spiking (label d) owing to resonance properties. The rebound spike in stellate cell $S_{T2}1$ activates a different interneuron $I_{T1}1$ (label e), causing inhibition in the first stellate cell. This initiates a rebound spike that starts the same cycle again. Note that the spikes in the stellate cells S_{T1} and S_{T2} fall on alternating cycles, similar to experimental data on theta cycle skipping [17,40,41] or data showing different populations active on opposite phases of theta [62]. Thus, theta cycle skipping suggests a specific mechanism for maintenance of network activity. In the figures, medial septum input was designed to use theta cycle skipping consistent with data [42,43], but in these simulations the network can effectively generate theta cycle skipping even if the medial septal input is at theta rhythm frequency.

By contrast, simulations with synchronous activation of these cells do not allow self-sustained cycle skipping (not shown). With synchronous activation, the feedback inhibition arrives during the fast afterhyperpolarization immediately after spiking and does not induce rebound spiking in other neurons. Therefore, using inhibitory rebound for self-sustained network activity appears to require the presence of theta cycle skipping in the network [17,40,41]. By contrast, excitatory interactions could occur on the same cycle, as they push the already active neuron to spike more on the same cycle, thereby enhancing depolarization and triggering stronger rebound on the next cycle. Evidence indicates that stellate cells do not have excitatory reciprocal connections [63] but it is possible that they have excitatory interactions with pyramidal cells in other layers.

The theta cycle skipping model can shift the spiking activity between different neurons, as shown in figure 3. If the timing of rebound from inhibition matches the timing of medial septal input to the interneuron of the same index (figure 3*a*), then the network spiking activity stably persists in a single pair of stellate cells (and interneurons), but if the timing of rebound from inhibition is faster than the time to the next theta cycle input to the interneurons, then the rebound spiking occurs in phase with the phasic input to a different interneuron, resulting in a shift in the spiking activity to different pairs of stellate cells and interneurons at a rate in proportion to the difference in timing of rebound spiking (figure 3*b*). In this example, a difference in running speed is represented by a change in the magnitude of inhibitory synaptic input to the stellate cells, but can also be implemented as a change in frequency of medial septal input or as a change in the intrinsic time course of rebound spiking.

7. Intrinsic rebound spiking and resonance frequency influence grid field spacing

As shown in figure 3*c*,*d*, the spiking model was used to generate plots of the spatially periodic firing of a stellate cell as a rat runs different distances at different speeds in different directions along a linear track. This demonstrates that the model can generate a consistent spatial location of firing despite changes in direction and running speed, and shows how differences in spacing of firing fields can result from a change in a single parameter of the spiking model (parameter a in equation (4.6)). The model shown in figure 3*c*(i),*d*(i),*e*(i),*f*(i) has parameter $a = 0.015$, that causes a faster rebound spike in response to a 10 ms hyperpolarizing current injection (figure 3*f*(i)), as well as a higher resonant frequency in response to a chirp function current injection (figure 3*e*(i)) compared to traces with $a = 0.01$. Because of the faster rebound, the activity in this network correspondingly transitioned more rapidly between different neurons (figure 3*c*(i)), and therefore generated spatial firing patterns with narrower spacing between firing fields (figure 3*d*(i)). By contrast, setting the spiking neuron parameter to $a = 0.01$ resulted in slower rebound spiking (figure 3*f*(ii)) and a lower resonant frequency (figure 3*e*(ii)). Without any other difference in the simulation, setting $a = 0.01$ resulted in slower transitions between neurons (figure 3*c*(ii)), and therefore wider spacing between firing fields (figure 3*d*(ii)). Inconsistencies in spacing occurred at some speeds, possibly owing to the inconsistencies in rebound timing relative to discrete medial septum input phases.

As shown in figure 3, a change in parameters in the spiking model that causes a difference in resonance frequency and speed of rebound spiking causes a change in spacing of grid cell firing fields. Thus, the model addresses how the spatial scale of grid cells could depend upon the difference in resonance frequency of stellate cells at different dorsal to ventral positions in medial entorhinal cortex [31]. The model also shows how the decrease in resonance frequency caused by cholinergic modulation of stellate cells [46,49] could contribute to the increase in size and spacing of grid cell firing fields

observed in rats foraging in novel environments [48,49]. The model also shows how the presence of low frequency resonance could underlie the generation of grid cells with larger size and spacing that are described in HCN1 knockout mice [51]. In the model, a difference in spacing can be obtained by shifting only a single intrinsic parameter influencing the intrinsic rebound spiking and resonant frequency of stellate cells. This provides an alternative to other possible mechanisms of grid field spacing, for example differences in the slope of the velocity-dependent change in frequency of medial septal input.

8. Response to running speed

Figure 3 shows plots of oscillatory activity switching between different populations over time as the simulated rat runs in different directions at progressively different speeds. To simulate consistent firing relative to spatial location, the model must simulate the running speed of a rat during exploration. This running speed must influence the relative duration of two intervals in the network: the interval between rebound spikes versus the interval of each cycle of medial septum input. One way this can be done is by altering the intrinsic resonance frequency and speed of rebound in stellate cells, possibly by giving different levels of baseline depolarization. Consistent with this, subthreshold resonance changes frequency with depolarization [37], though subthreshold oscillations do not [64]. In this manner, the resonance frequency could be adjusted by depolarization in proportion to movement direction and running speed. As an alternative, the model works well if running speed causes changes in the frequency of medial septal input. A change in frequency of medial septal input was used in a model using oscillatory ring attractors [6], which has been supported by data showing changes in frequency of theta cells dependent upon movement direction and speed [28]. In the simulations in the electronic supplementary material, figure S1, faster shifts in firing field occur if resonance stays the same but medial septal input frequency is reduced, thereby increasing the difference in frequency. However, this raises problems as running speed normally causes an increase in network theta frequency [65]. If medial septal input frequency were higher than resonant frequency, this would also cause shifts in firing fields but would result in precession of spiking in the wrong direction unless the medial septal input goes directly to stellate cells and interacts with a slower rebound mechanism. As the third alternative, simulations in the spiking model in figure 3*c*,*d* (and figure 4) show that increasing the strength of input from inhibitory interneurons to stellate cells in the model systematically increases the rate of transition between populations, matching an increase in velocity. The change in inhibitory input could be provided by having a population of neurons between the stellate cells and interneurons with varying levels of activity, thereby regulating the magnitude of feedback inhibition. Figure 3 shows that the model has the capacity to maintain spatially selective firing location despite changes in running speed and changes in direction on a one-dimensional track. The faster transition with larger inhibition could contribute to the narrower spacing of grid cell firing fields in dorsal medial entorhinal cortex because inhibition has been shown to be stronger and broader in dorsal versus ventral medial entorhinal cortex [66].

9. Resonance and rebound dynamics resemble oscillatory interference

As shown in the simulations, the resonance and rebound model presented here can generate the periodic beat patterns that are characteristics of oscillatory interference models [3–5]. As shown in the electronic supplementary material, figure S1, individual neurons show progressive shifts in amplitude of oscillations and the overall activity shifts between different neurons in the population. As in the oscillatory interference models, these beat patterns arise from a difference in relative frequency, in this case between the resonance frequency (determining rebound speed) of stellate cells and the medial septal input frequency. However, note that in contrast to most oscillatory interference models, the beat patterns in this model will only appear if there are competing oscillators. A single circuit will either stop firing or converge to a steady frequency. The competition between circuits with different phases has the effect of reducing the range of theta phase precession in the model in figures 2 and 3. Those models exhibit precession of spiking activity across 90° or less of the theta cycle. By contrast, theta phase precession across a wider range of phases was obtained in figure 4 by using a single inhibitory interneuron interacting with each stellate population (in contrast to using populations of inhibitory interneurons receiving phasic medial septal input as in figure 3). The overall functional properties of the network in figure 4 are similar to figure 3, but figure 4 has a much larger phase range over which stellate cells are active, resulting in substantial phase precession relative to the phase of medial septal input (figure 4*d*(i)c,(ii)c).

As shown in figures 3 and 4, the method of combining neurons with inhibitory interactions to cause rebound spiking provides an interesting functional rationale for the presence of theta cycle skipping in neurons of medial entorhinal cortex [17,40,41]. In addition, this model avoids the problem of the unreliable nature of subthreshold oscillations by directly focusing on the resonance properties and rebound timing shown to be highly reliable and deterministic in studies of medial entorhinal layer II neurons [29–31,33,46,50,58]. The model cannot maintain spatially selective firing without the medial septal input providing a phase signal. Reduction or removal of medial septal input results in static firing patterns or firing throughout the network (not shown). In this way, the model addresses recent data showing the loss of the spatial periodicity of grid cells when network theta rhythm oscillations are reduced by inactivation of the medial septum [10,11].

Addition of feedback excitation between the stellate cells and pyramidal cells in the model could give attractor dynamics coupled with resonance that could overcome problems with variability in spike timing similar to other models that use interactions of network oscillations [67]. The network dynamics used here overcome some issues preventing implementation of oscillatory interference with single neurons, including the variability of the temporal period of membrane potential oscillations or bistable persistent spiking [68] and the tendency of different oscillations within single neurons to synchronize [69,70].

The properties of resonance could be used in attractor models of grid cells. The model presented here shows how the intrinsic properties of individual neurons could help to maintain activity during low firing rates and theta rhythmic

spiking. Intrinsic properties relevant to this mechanism include *h* current dynamics underlying resonance that can generate rebound spiking. Another mechanism using intrinsic properties of neurons involves the calcium-activated non-specific cation (CAN) current that can generate an afterdepolarization after spiking and can underlie bistability of spiking activity in some conditions [71,72]. The CAN current can cause generation of spiking that depends upon calcium influx caused by a previous spike. The properties of the CAN current in causing cyclical increases and decreases in spiking activity [73,74] were previously proposed to underlie the generation of grid cell firing properties [75,76]. On a faster time-scale, the self-sustained spiking generated by the CAN current [71,72] could provide a spike interval phase code to generate grid cell firing [7], but this suffers from the problem of variability in spike times [68]. The generation of an afterdepolarization that generates spikes after a previous spike has been used in a model [56] that combines attractor dynamics with theta phase precession, but that model did not address subthreshold membrane potential resonance or rebound from inhibition.

Previous models have not addressed the functional role of data showing theta cycle skipping in medial entorhinal cortex neurons [17,40,41], or the data showing that cross-correlations of theta cycle skipping depend upon the functional tuning properties of conjunctive grid cells and head direction cells [41]. This new model also has the benefit of addressing the loss of the spatial periodicity of grid cells when network theta rhythm oscillations are reduced by inactivation of the medial septum [10,11].

Both models using attractor dynamics and models using oscillatory interference employ a simple representation of velocity that does not address all features of the physiological data including the fact that the speed modulation of firing is often separate from the directional tuning of cells. Both types of models use movement direction as a component of velocity, but recent data show that despite many medial entorhinal cells being tuned to head direction, only a few are tuned to movement direction [77]. The predominance of head direction sensitivity in medial entorhinal cortex rather than movement direction sensitivity suggests an important role of grid cells in monitoring the angle of sensory input, which requires keeping track of head direction. The grid cells and other functional neurons in medial entorhinal cortex may interface this sensory input with path integration [78]. The path integration may primarily depend on input from neurons shown to be sensitive to movement direction in the medial septum and thalamus [28]. This supports a model related to oscillatory interference in which oscillating rings of theta cells could provide phasic input to regulate grid cell firing [6,28]. There is an important question of how the phase of the oscillating rings could be influenced by the timing of spikes owing to the difference in intrinsic resonance properties at different dorsal–ventral positions to influence the spacing of grid cell firing fields. This could be obtained if the phase and amplitude of oscillations of each ring were updated by the circular mean phase and mean amplitude relative to the directional preference of that ring for all of the active grid cells in the entorhinal cortex, as done in a previous grid cell model [76]. This may regulate the input from a large range of preferred directions to generate circularly symmetric interference that would generate hexagonal grid cell firing patterns and may also ensure that the rings have the correct phase relative to grid cell firing when the animal turns. The intrinsic properties could influence the spacing of grid cell firing fields if the pattern of spikes based on intrinsic properties influences the phase of medial septal input for multiple movement directions.

The determination of the mechanisms of grid cells will require continued modelling and new physiological experiments. This article briefly reviews a variant of the oscillatory interference model that potentially links the intrinsic resonance properties of neurons to grid cell firing and provides a circuit account for the potential role of theta cycle skipping in generating grid cell firing patterns. Different grid cell models effectively address different aspects of the experimental data and are not incompatible with each other. A model that accounts for the full range of data will likely combine elements of many of the current categories of grid cell models.

Funding statement. Research supported by NIHM R01 MH60013, R01 MH61492, Silvio O. Conte Center P50 MH094263 and the Office of Naval Research MURI grant no. N00014-10-1-0936.

References

1. Moser EI, Moser MB. 2008 A metric for space. *Hippocampus* **18**, 1142–1156. (doi:10.1002/hipo.20483)
2. Fyhn M, Molden S, Witter MP, Moser EI, Moser MB. 2004 Spatial representation in the entorhinal cortex. *Science* **305**, 1258–1264. (doi:10.1126/science.1099901)
3. Burgess N, Barry C, Jeffery KJ, O'Keefe J. 2005 A grid and place cell model of path integration utilizing phase precession versus theta. Poster presented at the *Computational Cognitive Neuroscience Conference, Washington DC, 10–11 November 2005*. See http://cdn.f1000.com/posters/docs/225.
4. Burgess N, Barry C, O'Keefe J. 2007 An oscillatory interference model of grid cell firing. *Hippocampus* **17**, 801–812. (doi:10.1002/hipo.20327)
5. Burgess N. 2008 Grid cells and theta as oscillatory interference: theory and predictions. *Hippocampus* **18**, 1157–1174. (doi:10.1002/hipo.20518)
6. Blair HT, Gupta K, Zhang K. 2008 Conversion of a phase- to a rate-coded position signal by a three-stage model of theta cells, grid cells, and place cells. *Hippocampus* **18**, 1239–1255. (doi:10.1002/hipo.20509)
7. Hasselmo ME. 2008 Grid cell mechanisms and function: contributions of entorhinal persistent spiking and phase resetting. *Hippocampus* **18**, 1213–1229. (doi:10.1002/hipo.20512)
8. Hafting T, Fyhn M, Bonnevie T, Moser MB, Moser EI. 2008 Hippocampus-independent phase precession in entorhinal grid cells. *Nature* **453**, 1248–1252. (doi:10.1038/nature06957)
9. Jeewajee A, Barry C, O'Keefe J, Burgess N. 2008 Grid cells and theta as oscillatory interference: electrophysiological data from freely moving rats. *Hippocampus* **18**, 1175–1185. (doi:10.1002/hipo.20510)
10. Brandon MP, Bogaard AR, Libby CP, Connerney MA, Gupta K, Hasselmo ME. 2011 Reduction of theta rhythm dissociates grid cell spatial periodicity from directional tuning. *Science* **332**, 595–599. (doi:10.1126/science.1201652)
11. Koenig J, Linder AN, Leutgeb JK, Leutgeb S. 2011 The spatial periodicity of grid cells is not sustained during reduced theta oscillations. *Science* **332**, 592–595. (doi:10.1126/science.1201685)
12. Stensola H, Stensola T, Solstad T, Froland K, Moser MB, Moser EI. 2012 The entorhinal grid map is discretized. *Nature* **492**, 72–78. (doi:10.1038/nature11649)
13. Climer JR, Newman EL, Hasselmo ME. 2013 Phase coding by grid cells in unconstrained environments:

two-dimensional phase precession. *Eur. J. Neurosci.* **38**, 2526–2541. (doi:10.1111/ejn.12256)

14. Mitchell SJ, Ranck Jr JB. 1980 Generation of theta rhythm in medial entorhinal cortex of freely moving rats. *Brain Res.* **189**, 49–66. (doi:10.1016/0006-8993(80)90006-2)
15. Mitchell SJ, Rawlins JN, Steward O, Olton DS. 1982 Medial septal area lesions disrupt theta rhythm and cholinergic staining in medial entorhinal cortex and produce impaired radial arm maze behavior in rats. *J. Neurosci.* **2**, 292–302.
16. Alonso A, Garcia-Austt E. 1987 Neuronal sources of theta rhythm in the entorhinal cortex of the rat. I. Laminar distribution of theta field potentials. *Exp. Brain Res.* **67**, 493–501. (doi:10.1007/BF00247282)
17. Jeffery KJ, Donnett JG, O'Keefe J. 1995 Medial septal control of theta-correlated unit firing in the entorhinal cortex of awake rats. *Neuroreport* **6**, 2166–2170. (doi:10.1097/00001756-199511000-00017)
18. Fuhs MC, Touretzky DS. 2006 A spin glass model of path integration in rat medial entorhinal cortex. *J. Neurosci.* **26**, 4266–4276. (doi:10.1523/JNEUROSCI.4353-05.2006)
19. McNaughton BL, Battaglia FP, Jensen O, Moser EI, Moser MB. 2006 Path integration and the neural basis of the 'cognitive map'. *Nat. Rev. Neurosci.* **7**, 663–678. (doi:10.1038/nrn1932)
20. Guanella A, Kiper D, Verschure P. 2007 A model of grid cells based on a twisted torus topology. *Int. J. Neural Syst.* **17**, 231–240. (doi:10.1142/S0129065707001093)
21. Burak Y, Fiete IR. 2009 Accurate path integration in continuous attractor network models of grid cells. *PLoS Comput. Biol.* **5**, e1000291. (doi:10.1371/journal.pcbi.1000291)
22. Sargolini F, Fyhn M, Hafting T, McNaughton BL, Witter MP, Moser MB, Moser EI. 2006 Conjunctive representation of position, direction, and velocity in entorhinal cortex. *Science* **312**, 758–762. (doi:10.1126/science.1125572)
23. Barry C, Hayman R, Burgess N, Jeffery KJ. 2007 Experience-dependent rescaling of entorhinal grids. *Nat. Neurosci.* **10**, 682–684. (doi:10.1038/nn1905)
24. Kropff E, Treves A. 2008 The emergence of grid cells: intelligent design or just adaptation? *Hippocampus* **18**, 1256–1269. (doi:10.1002/hipo.20520)
25. Mhatre H, Gorchetchnikov A, Grossberg S. 2010 Grid cell hexagonal patterns formed by fast self-organized learning within entorhinal cortex. *Hippocampus* **22**, 320–334. (doi:10.1002/hipo.20901)
26. Si B, Kropff E, Treves A. 2012 Grid alignment in entorhinal cortex. *Biol. Cybern.* **106**, 483–506. (doi:10.1007/s00422-012-0513-7)
27. Bonnevie T, Dunn B, Fyhn M, Hafting T, Derdikman D, Kubie JL, Roudi Y, Moser EI, Moser M-B. 2013 Grid cells require excitatory drive from the hippocampus. *Nat. Neurosci.* **16**, 309–317. (doi:10.1038/nn.3311)
28. Welday AC, Shlifer IG, Bloom ML, Zhang K, Blair HT. 2011 Cosine directional tuning of theta cell burst frequencies: evidence for spatial coding by oscillatory interference. *J. Neurosci.* **31**, 16 157–16 176. (doi:10.1523/JNEUROSCI.0712-11.2011)
29. Haas JS, White JA. 2002 Frequency selectivity of layer II stellate cells in the medial entorhinal cortex. *J. Neurophysiol.* **88**, 2422–2429. (doi:10.1152/jn.00598.2002)
30. Erchova I, Kreck G, Heinemann U, Herz AV. 2004 Dynamics of rat entorhinal cortex layer II and III cells: characteristics of membrane potential resonance at rest predict oscillation properties near threshold. *J. Physiol.* **560**, 89–110. (doi:10.1113/jphysiol.2004.069930)
31. Giocomo LM, Zilli EA, Fransen E, Hasselmo ME. 2007 Temporal frequency of subthreshold oscillations scales with entorhinal grid cell field spacing. *Science* **315**, 1719–1722. (doi:10.1126/science.1139207)
32. Giocomo LM, Hasselmo ME. 2008 Computation by oscillations: implications of experimental data for theoretical models of grid cells. *Hippocampus* **18**, 1186–1199. (doi:10.1002/hipo.20501)
33. Boehlen A, Heinemann U, Erchova I. 2010 The range of intrinsic frequencies represented by medial entorhinal cortex stellate cells extends with age. *J. Neurosci.* **30**, 4585–4589. (doi:10.1523/JNEUROSCI.4939-09.2010)
34. Pastoll H, Ramsden HL, Nolan MF. 2012 Intrinsic electrophysiological properties of entorhinal cortex stellate cells and their contribution to grid cell firing fields. *Front. Neural Circuits* **6**, 17. (doi:10.3389/fncir.2012.00017)
35. Canto CB, Witter MP. 2012 Cellular properties of principal neurons in the rat entorhinal cortex. II. The medial entorhinal cortex. *Hippocampus* **22**, 1277–1299. (doi:10.1002/hipo.20993)
36. Canto CB, Witter MP. 2012 Cellular properties of principal neurons in the rat entorhinal cortex. I. The lateral entorhinal cortex. *Hippocampus* **22**, 1256–1276. (doi:10.1002/hipo.20997)
37. Shay CF, Boardman IS, James NM, Hasselmo ME. 2012 Voltage dependence of subthreshold resonance frequency in layer II of medial entorhinal cortex. *Hippocampus* **22**, 1733–1749. (doi:10.1002/hipo.22008)
38. Alonso A, Klink R. 1993 Differential electroresponsiveness of stellate and pyramidal-like cells of medial entorhinal cortex layer II. *J. Neurophysiol.* **70**, 128–143.
39. Alonso A, Llinas RR. 1989 Subthreshold Na-dependent theta-like rhythmicity in stellate cells of entorhinal cortex layer II. *Nature* **342**, 175–177. (doi:10.1038/342175a0)
40. Deshmukh SS, Yoganarasimha D, Voicu H, Knierim JJ. 2010 Theta modulation in the medial and the lateral entorhinal cortices. *J. Neurophysiol.* **104**, 994–1006. (doi:10.1152/jn.01141.2009)
41. Brandon MP, Bogaard AR, Schultheiss NW, Hasselmo ME. 2013 Segregation of cortical head direction cell assemblies on alternating theta cycles. *Nat. Neurosci.* **16**, 739–748. (doi:10.1038/nn.3383)
42. King C, Reece M, O'Keefe J. 1998 The rhythmicity of cells of the medial septum/diagonal band of Broca in the awake freely moving rat: relationships with behaviour and hippocampal theta. *Eur. J. Neurosci.* **10**, 464–477. (doi:10.1046/j.1460-9568.1998.00026.x)
43. Varga V, Hangya B, Kranitz K, Ludanyi A, Zemankovics R, Katona I, Shigemoto R, Freund TF, Borhegyi Z. 2008 The presence of pacemaker HCN channels identifies theta rhythmic GABAergic neurons in the medial septum. *J. Physiol.* **586**, 3893–3915. (doi:10.1113/jphysiol.2008.155242)
44. Hafting T, Fyhn M, Molden S, Moser MB, Moser EI. 2005 Microstructure of a spatial map in the entorhinal cortex. *Nature* **436**, 801–806. (doi:10.1038/nature03721)
45. Hargreaves EL, Rao G, Lee I, Knierim JJ. 2005 Major dissociation between medial and lateral entorhinal input to dorsal hippocampus. *Science* **308**, 1792–1794. (doi:10.1126/science.1110449)
46. Heys JG, Giocomo LM, Hasselmo ME. 2010 Cholinergic modulation of the resonance properties of stellate cells in layer II of medial entorhinal cortex. *J. Neurophysiol.* **104**, 258–270. (doi:10.1152/jn.00492.2009)
47. Acquas E, Wilson C, Fibiger HC. 1996 Conditioned and unconditioned stimuli increase frontal cortical and hippocampal acetylcholine release: effects of novelty, habituation, and fear. *J. Neurosci.* **16**, 3089–3096.
48. Barry C, Ginzberg LL, O'Keefe J, Burgess N. 2012 Grid cell firing patterns signal environmental novelty by expansion. *Proc. Natl Acad. Sci. USA* **109**, 17 687–17 692. (doi:10.1073/pnas.1209918109)
49. Barry C, Heys JG, Hasselmo ME. 2012 Possible role of acetylcholine in regulating spatial novelty effects on theta rhythm and grid cells. *Front. Neural Circuits* **6**, 5. (doi:10.3389/fncir.2012.00005)
50. Giocomo LM, Hasselmo ME. 2009 Knock-out of HCN1 subunit flattens dorsal–ventral frequency gradient of medial entorhinal neurons in adult mice. *J. Neurosci.* **29**, 7625–7630. (doi:10.1523/JNEUROSCI.0609-09.2009)
51. Giocomo LM, Hussaini SA, Zheng F, Kandel ER, Moser MB, Moser EI. 2011 Grid cells use HCN1 channels for spatial scaling. *Cell* **147**, 1159–1170. (doi:10.1016/j.cell.2011.08.051)
52. Heys JG, MacLeod KM, Moss CF, Hasselmo ME. 2013 Bat and rat neurons differ in theta-frequency resonance despite similar coding of space. *Science* **340**, 363–367. (doi:10.1126/science.1233831)
53. Yartsev MM, Witter MP, Ulanovsky N. 2011 Grid cells without theta oscillations in the entorhinal cortex of bats. *Nature* **479**, 103–107. (doi:10.1038/nature10583)
54. Guanella A, Verschure PF. 2007 Prediction of the position of an animal based on populations of grid and place cells: a comparative simulation study. *J. Integr. Neurosci.* **6**, 433–446. (doi:10.1142/S0219635207001556)
55. Pastoll H, Solanka L, van Rossum MC, Nolan MF. 2013 Feedback inhibition enables theta-nested gamma oscillations and grid firing fields. *Neuron* **77**, 141–154. (doi:10.1016/j.neuron.2012.11.032)
56. Navratilova Z, Giocomo LM, Fellous JM, Hasselmo ME, McNaughton BL. 2012 Phase precession and variable spatial scaling in a periodic attractor map

model of medial entorhinal grid cells with realistic after-spike dynamics. *Hippocampus* **22**, 772–789. (doi:10.1002/hipo.20939)

57. Dickson CT, Mena AR, Alonso A. 1997 Electroresponsiveness of medial entorhinal cortex layer III neurons in vitro. *Neuroscience* **81**, 937–950. (doi:10.1016/S0306-4522(97)00263-7)
58. Engel TA, Schimansky-Geier L, Herz AV, Schreiber S, Erchova I. 2008 Subthreshold membrane-potential resonances shape spike-train patterns in the entorhinal cortex. *J. Neurophysiol.* **100**, 1576–1589. (doi:10.1152/jn.01282.2007)
59. Schreiber S, Erchova I, Heinemann U, Herz AV. 2004 Subthreshold resonance explains the frequency-dependent integration of periodic as well as random stimuli in the entorhinal cortex. *J. Neurophysiol.* **92**, 408–415. (doi:10.1152/jn.01116.2003)
60. Izhikevich EM. 2007 *Dynamical systems in neuroscience: the geometry of excitability and bursting*, p. 315. Cambridge, MA: MIT Press.
61. Blair HT, Wu A, Cong J. 2014 Oscillatory neurocomputing with ring attractors: a network architecture for mapping locations in space onto patterns of neural synchrony. *Phil. Trans. R. Soc. B* **369**, 20120526. (doi:10.1098/rstb.2012.0526)
62. Mizuseki K, Sirota A, Pastalkova E, Buzsaki G. 2009 Theta oscillations provide temporal windows for local circuit computation in the entorhinal-hippocampal loop. *Neuron* **64**, 267–280. (doi:10.1016/j.neuron.2009.08.037)
63. Couey JJ *et al*. 2013 Recurrent inhibitory circuitry as a mechanism for grid formation. *Nat. Neurosci.* **16**, 318–324. (doi:10.1038/nn.3310)
64. Yoshida M, Giocomo LM, Boardman I, Hasselmo ME. 2011 Frequency of subthreshold oscillations at different membrane potential voltages in neurons at different anatomical positions on the dorsoventral axis in the rat medial entorhinal cortex. *J. Neurosci.* **31**, 12 683–12 694. (doi:10.1523/JNEUROSCI.1654-11.2011)
65. Hinman JR, Penley SC, Long LL, Escabi MA, Chrobak JJ. 2010 Septotemporal variation in dynamics of theta: speed and habituation. *J. Neurophysiol.* **105**, 2675–2686. (doi:10.1152/jn.00837.2010)
66. Beed P, Gundlfinger A, Schneiderbauer S, Song J, Bohm C, Burgalossi A, Brecht M, Vida I, Schmitz D. 2013 Inhibitory gradient along the dorsoventral axis in the medial entorhinal cortex. *Neuron* **79**, 1197–1207. (doi:10.1016/j.neuron.2013.06.038)
67. Zilli EA, Hasselmo ME. 2010 Coupled noisy spiking neurons as velocity-controlled oscillators in a model of grid cell spatial firing. *J. Neurosci.* **30**, 13 850–13 860. (doi:10.1523/JNEUROSCI.0547-10.2010)
68. Zilli EA, Yoshida M, Tahvildari B, Giocomo LM, Hasselmo ME. 2009 Evaluation of the oscillatory interference model of grid cell firing through analysis and measured period variance of some biological oscillators. *PLoS Comput. Biol.* **5**, e1000573. (doi:10.1371/journal.pcbi.1000573)
69. Remme MW, Lengyel M, Gutkin BS. 2009 The role of ongoing dendritic oscillations in single-neuron dynamics. *PLoS Comput. Biol.* **5**, e1000493. (doi:10.1371/journal.pcbi.1000493)
70. Remme MW, Lengyel M, Gutkin BS. 2010 Democracy-independence trade-off in oscillating dendrites and its implications for grid cells. *Neuron* **66**, 429–437. (doi:10.1016/j.neuron.2010.04.027)
71. Egorov AV, Hamam BN, Fransen E, Hasselmo ME, Alonso AA. 2002 Graded persistent activity in entorhinal cortex neurons. *Nature* **420**, 173–178. (doi:10.1038/nature01171)
72. Fransén E, Tahvildari B, Egorov AV, Hasselmo ME, Alonso AA. 2006 Mechanism of graded persistent cellular activity of entorhinal cortex layer v neurons. *Neuron* **49**, 735–746. (doi:10.1016/j.neuron.2006.01.036)
73. Klink R, Alonso A. 1997 Muscarinic modulation of the oscillatory and repetitive firing properties of entorhinal cortex layer II neurons. *J. Neurophysiol.* **77**, 1813–1828.
74. Klink R, Alonso A. 1997 Ionic mechanisms of muscarinic depolarization in entorhinal cortex layer II neurons. *J. Neurophysiol.* **77**, 1829–1843.
75. Hasselmo ME, Brandon MP. 2008 Linking cellular mechanisms to behavior: entorhinal persistent spiking and membrane potential oscillations may underlie path integration, grid cell firing, and episodic memory. *Neural Plast.* **2008**, 658323. (doi:10.1155/2008/658323)
76. Hasselmo ME, Brandon MP. 2012 A model combining oscillations and attractor dynamics for generation of grid cell firing. *Front. Neural Circuits* **6**, 30. (doi:10.3389/fncir.2012.00030)
77. Raudies F, Chapman GW, Brandon MP, Hasselmo ME. 2013 Movement direction is not coded by the firing of most entorhinal cells but is required by grid cell models. *Soc. Neurosci. Abstr.* **39**, 696.11.
78. Milford MJ, Wiles J, Wyeth GF. 2010 Solving navigational uncertainty using grid cells on robots. *PLoS Comput. Biol.* **6**, e1000995. (doi:10.1371/journal.pcbi.1000995)